Temperatures of Ancient Eclogites Estimated Using Zirconium-in-Rutile Geothermometry

Audrey Graham

Advisor: Dr. Sarah Penniston-Dorland

GEOL394

University of Maryland, College Park, USA

Abstract

The Kuru-Vaara and Gridino samples from the Belomorian Province in eastern Russia are eclogites that represent an ancient subduction zone. These samples experienced high-temperature and high-pressure metamorphism during subduction and are useful for making comparisons to modern subduction zones to find changes in metamorphism and subduction processes throughout Earth's history. In subduction zones, rocks will experience increasing temperatures and pressures with increasing depths. The rocks will then be brought back up to Earth's surface in a process known as exhumation, where they may encounter an increase in temperature before both pressure and temperature return to surface conditions. The peak temperatures experienced by the rock can be estimated using the zirconium-in-rutile method, which uses the concentration of zirconium within a rutile crystal to calculate temperature. However, during exhumation, high temperatures may cause the zirconium concentration of the rutile crystals to be reset, reflecting the elevated temperatures experienced during the rock's retrograde path. The shielding of rutile crystals by garnet crystals may allow the temperatures recorded during subduction to be preserved. Rutile crystals included within garnet have no contact with the matrix of the rock, which prevents the exchange reaction that allows the reequilibration of zirconium within rutile crystals. A comparison is made between the zirconium concentration of rutile crystals within the matrix versus rutile inclusions within garnet. This comparison can be used to determine whether the rutile crystals between these two locations record the same, or separate stages of the rock's metamorphism. The maximum zirconium concentration is obtained using the mean-max method, following the procedure outlined in Harvey et al. (2021). In the Kuru-Vaara sample, there was no difference in measured zirconium concentration between rutile crystals included within garnet (753 ± 230 ppm 2σ) versus within the matrix (607 ± 68 2σ). Similarly, in the Gridino sample, there was no difference in measured zirconium concentration between rutile crystals in garnet (1046 ± 311 ppm 2σ) versus within the matrix (539 ± 301 ppm 2σ). A traverse through a garnet crystal in the Kuru-Vaara sample reveals that zirconium concentrations decrease with increasing distance from the garnet's center, implying that rutile crystals within garnet record the rock's exhumation path.

Plain-Text Abstract

Subduction zones are a type of tectonic plate boundary that have an influence on Earth's processes, such as earthquakes, volcanoes, and the movement of tectonic plates. During subduction, rocks within the subducting plate are subjected to high temperatures and pressures. As temperature and pressure increase, the rock unit undergoes metamorphism, wherein minerals within the rock undergo changes in composition. These changes in composition can be useful for determining the conditions that these rocks have experienced; specifically, geothermometers such as zirconium-in-rutile can be used to calculate the temperatures that the rock experienced. The process of subduction may not have behaved the same way throughout the entirety of Earth's history. It is hypothesized that ancient subduction zones hotter than modern subduction zones. Investigating the temperatures recorded by rutile crystals within these rocks through the use of the zirconium-in-rutile geothermometer is a way to observe differences between ancient and modern subduction zones. In this geothermometer, the concentration of zirconium within rutile crystals can act as a proxy for temperatures that the rock has experienced during subduction. However, when subducted material is brought back up to Earth's surface, it may experience higher

temperatures than what it experienced during its subduction. In this situation the geothermometer may reset, and instead record the temperatures experienced during exhumation, rather than subduction. Minerals such as garnet have been hypothesized to be able to shield mineral inclusions such as rutile from being reset.

Table of Contents

Abstract 1
Plain-Text Abstract 1
Introduction 4
Hypotheses 5
Geologic Background 6
Belomorian Province 6
Previous Estimates of P-T Conditions 6
Methods 7
Zirconium-in Rutile-Geothermometry 7
Data Collection 8
Samples 9
Results 10
Discussion 15
Zirconium-in-Rutile Geothermometry 15
Garnet Traverse 15
Interpretation 16
Prograde vs. Retrograde Conditions 16
Potential for Future Work 18
Conclusions and Broader Impact 19
Acknowledgements 19
Bibliography 20
Appendices 22
Appendix A – EDS Spectra 22
Appendix B – Summary Table 22
Appendix C – Data 25
Appendix D – University Honor Code 0

Introduction

The subduction of crust is an influential and powerful Earth process that greatly influences the planet's tectonics, seismic activity, and volcanism. Subduction zones are a tectonic setting wherein tectonic plates converge, and one plate subducts under the other. The subducting plate is subject to intense heat and pressure, which causes the rocks present to metamorphose and transform. The investigation of these metamorphosed rocks allows for a greater understanding of tectonic processes in both Earth's present and past. The Earth is in a constant state of flux; changes can occur along long time scales, and the behavior of Earth today may be different than it was billions of years ago. A better understanding of these processes and their relationships with other Earth processes can be obtained by investigating rock samples that have experienced and recorded conditions they experienced.

The rock samples that have been analyzed originate from a geologic unit that represents an ancient subduction zone of oceanic crust (Shchipansky et al., 2012). When oceanic crust is subducted and subjected to high pressures and elevated temperatures, the rocks that make up this crust are transformed in terms of their structure and their mineralogy. The transformation of the rock reflects the facies it was formed in. The samples that have been analyzed were formed in the eclogite facies and are composed mainly of the minerals garnet, omphacite, quartz, rutile, zircon. These samples are from the Belomorian Province, which is a rock unit containing eclogite. These Belomorian Province rocks are of interest due to their age. Age estimates are debated, but the oldest estimates for this subduction zone are 2.7 to 2.8 billion years old, which makes these rocks among the oldest subduction zone rocks that are being researched (Li et al, 2020). Earth's subduction zones have undergone many changes throughout the duration of Earth's existence; in particular, the temperature conditions of subduction zones have been found to have evolved over time, with older subduction zones exhibiting higher temperatures (Brown et al., 2022). In order to conduct research on these ancient subduction zones and temperatures that they have experienced during subduction, rocks that originate from these subduction zones may be investigated, including Belomorian Province rocks.

Subduction zones, while still experiencing elevated temperatures and pressure, are referred to as "cold" due to their low temperatures in comparison to other tectonic settings (Syracuse et al., 2010). This is because, as the subducting plate sinks into the Earth's hot mantle, its rate of subduction is faster than the rate at which heat can conduct through the plate (Syracuse et al., 2010). Nonetheless, as the plate is subducted, it will experience the growth of crystals along this pressure and temperature gradient. This path of increasing pressures and temperatures is known as the prograde path of the rock. On this prograde path, there exist different facies that represent different pressure-temperature conditions and exhibit different mineral assemblages. These minerals can record the temperatures that they have experienced during their crystallization. The Belomorian Province eclogite samples contain rutile crystals, which can be used as a geothermometer.

The method of analysis used to determine the peak metamorphic temperatures experienced by these rocks is the zirconium-in-rutile method. This method relies on the positive correlation between zirconium concentration in rutile and temperature (Zack et al, 2004; Kohn, 2020). This is because, as temperature increases within a rock, the cation site of the rutile can accommodate larger-sized cations, particularly zirconium (Zack et al., 2004; Kohn, 2020). The concentration of

zirconium within these rutile crystals is measured using the University of Maryland's Electron Probe Microanalyzer. The data points collected during analysis, each of which represents a different rutile crystal, are then used to estimate the temperatures that the rock has experienced.

These rocks have not only been subject to increasing temperatures and pressures during their subduction, but also retrogressive processes as they were exhumed back onto the surface of Earth. During this exhumation from depth, while the rock will experience a decrease in pressure, it may also experience a temperature increase before eventually reaching surface conditions (Van Keken et al., 2018). Consequently, the peak temperatures that are recorded by rutile crystals may not reflect the temperatures experienced during the rock's prograde path. Rather, they may instead record the high temperatures experienced during the retrogressive processes experienced during the exhumation of the rock. This effect is known as resetting, where the temperatures recorded by the crystal during prograde growth are reset during retrogression, and temperatures at shallower depths are instead recorded. This form of alteration can theoretically be mitigated by taking measurements from rutile crystals trapped within garnet crystals present in the rock. Like rutile crystals, garnet crystals experience continuous growth throughout the rock's metamorphic path. As the garnet experiences this continued growth, it will trap mineral inclusions within it, such as rutile crystals. Therefore, there will theoretically be rutile crystals included within the garnet crystal that have been shielded from alteration by retrogressive processes, and, therefore, will retain the temperatures recorded during the rock's subduction. These temperatures are compared to temperatures recorded by rutile crystals in the surrounding matrix, which would be prone to resetting during retrogression.

Hypotheses

The purpose of this analysis is to determine whether the concentration of zirconium within rutile crystals included in garnet crystals is different from the zirconium concentration of the rutile crystals within the matrix. The null hypothesis is as stated: concentrations of zirconium within rutile crystals included within a garnet will be the same as the zirconium concentrations of rutile crystals within the matrix of the eclogite. Therefore, the alternative hypothesis is stated as: the zirconium concentrations of rutile crystals included within garnet will be different than concentrations of zirconium within the matrix. As the concentration of zirconium within rutile crystals is used as a proxy for temperature, the investigation of these hypotheses may allow for a comparison of temperatures recorded by rutile crystals included within garnet versus the temperatures recorded by rutile crystals in the matrix.

Geologic Background

Belomorian Province

Rocks of the Belomorian Province originate from an ancient subduction followed by continental collision, wherein oceanic crust was subducted, allowing the rock unit to be subjected to high pressures and temperatures (Li et al., 2020). They were collected from two locations in western Russia northwest of the White Sea. The Belomorian Province has not only been subject to eclogite facies metamorphism, but also retrogressive processes during their exhumation from depths to Earth's surface. In Figure 1, the Belomorian Province is outlined in red. The Belomorian Province, during its exhumation upwards towards the surface of the Earth, was thrust on top of the Karelian Province in the west (Li et al., 2020; Slabunov et al., 2021). Then, the Belomorian province was, itself, overthrust by fault complexes of the Kola Province in the East (Li et al., 2020; Slabunov et al., 2021).

Fig 1. Map of northern Europe and northwestern Russia. The Belomorian Province is outlined in red, and the sample collection sites are highlighted with yellow stars: Kuru-Vaara (KV) and Gridino (G) (Slabunov et al., 2021).

The age of the Belomorian Province is controversial, as there are several different estimates of the specific age of this rock unit. Estimates include: 2.87 Ga, ranging from 2.72-2.70 Ga, and even as young as 1.9 Ga (Li et al., 2020; Liu et al., 2017). Nonetheless, even with the variety in age estimates, the age of this rock unit is estimated to be much older than most other eclogites that have been previously studied (Li et al., 2020). Examining subduction zone rocks of this age can demonstrate how tectonic processes have undergone temperature changes throughout time and can be used to investigate a proposed decrease in subduction zone temperature conditions over time (Brown et al., 2022).

Previous Estimates of P-T Conditions

There are existing P-T conditions that have been estimated using Belomorian Province eclogites. Some of these conditions were estimated by Liu et al. (2017), with P-T paths calculated for Kuru-Vaara eclogite. The P-T path of the Gridino eclogite was estimated by Perchuk and Morgunova (2014). These P-T paths can be seen plotted on Figure 2(a), which is a graph from Liu et al. (2017) that depicts pressure temperature paths of multiple Belomorian Province eclogite samples, including Kuru-Vaara (red arrow and grey area) and Gridino (orange arrows). As is visible in this figure, both estimated P-T paths for these eclogite samples are clockwise, and

document retrogression. In addition, the retrograde P-T conditions estimated by Liu et al. (2017) were determined from using the alteration of kyanite to sapphirine + spinel + plagioclase as a P-T constraint indicating that these rocks experienced granulite facies conditions after their subduction. This finding is supported by Shchipansky et al. (2012) which also describes Belomorian Province eclogites as having experienced retrogression. In order to determine these P-T paths, these studies have used the major-element composition of rocks and minerals, which are more subject to resetting than trace elements such as zirconium (Kohn 2020).

In addition to P-T conditions recorded by Belomorian Province eclogites, subduction zone rocks from across the globe may also be used as a comparison. Figure 2(b) portrays a multitude of P-T conditions recorded by blueschist and eclogite samples; these P-T conditions span over a wide range of conditions (Penniston-Dorland et al., 2015).

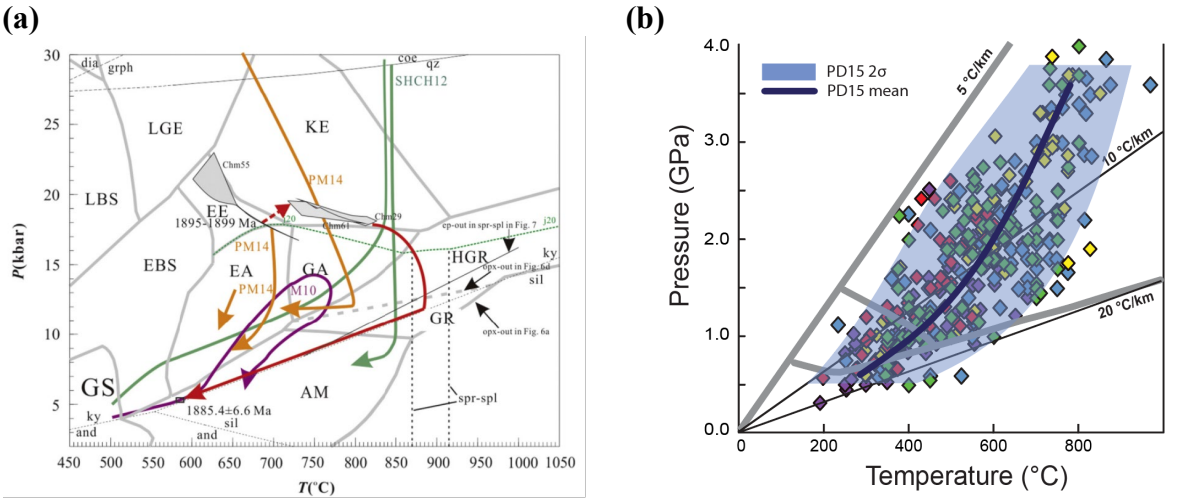

Fig 2. Previously estimated P-T conditions of subduction zones. **(a)** Graphed P-T paths of Belomorian Province rocks from Liu et al. (2017), including a P-T path for Kuru-Vaara (red arrow and grey area) and Gridino (orange) from Perchuk and Morgunova (2014). **(b)** Compilation of global P-T estimates from Penniston-Dorland et al. (2015).

Methods

Zirconium-in Rutile-Geothermometry

As the subducting plate experiences increasing pressure and temperature along its prograde path, there is a continual crystallization of rutile crystals. These rutile crystals are able to record the highest temperatures that they have experienced. This record is obtained because the cation site in rutile (which is typically occupied by titanium) is able to accommodate large ions like zirconium, meaning that there is a positive relationship between temperature and zirconium concentration within the rutile crystal (Zack et al., 2004). This means that, as rutile crystals experience elevated temperatures, the zirconium concentration within the rutile will increase as

well. This substitution of zirconium in the cation site of rutile is made possible by the exchange reaction that exists between zircon, α-quartz, and zirconium oxide within rutile:

$$ZrSiO_4 = SiO_2 + ZrO_2$$

(Kohn 2020)

The mineral α-quartz is in this exchange reaction rather than β-quartz because these eclogite samples formed in conditions within the α-quartz stability field. The use of zirconium-in-rutile geothermometry relies on this exchange reaction, and, therefore, can only be used in samples that contain both quartz and zircon (Zack et al., 2004). In the Kuru-Vaara sample, quartz and zircon were located both in the garnet and in the matrix. EDS Spectra of these minerals can be found in Appendix A.

The zirconium-in-rutile method uses measurements of zirconium concentration to calculate the peak temperature experienced by the rutile. In addition to zirconium concentration, this method also requires an estimate of pressure in order to calculate temperature. The specific pressure that has been experienced by these samples is unknown, so a range of pressures is used to calculate a possible range of temperatures that the rock has experienced. The equation used to calculate the temperatures experienced using zirconium concentration (C) and pressure (P) is as follows:

$$T(\mathrm{C}^\circ) = \frac{71360 + 0.378 \cdot P(\mathrm{bars}) - 0.130 \cdot C(\mathrm{ppm})}{130.66 - R \cdot \ln\left[C(\mathrm{ppm})\right]} - 273.1$$

(Kohn 2020)

Data Collection

An Electron Probe Microanalyzer (EPMA) is used for the collection of concentration data; the instrument, a JEOL 8900, is in the AIM Laboratory at the University of Maryland. Concentration data of several elements within these rutile crystals is collected. The machine operates by accelerating a beam of electrons focused to 1μm diameter on the mineral phase of interest. The accelerating voltage of the beam is 20 kV, and the sample current is 120 nA. When collecting data, the ZAF algorithm is used to determine concentrations of titanium, aluminum, iron, niobium, silicon, and zirconium. The purpose of using the ZAF algorithm is to correct for differences in atomic number, absorption of other elements, and fluorescence of other elements. The concentration of SiO_2 is used as a discriminant to determine whether the analysis was performed in a region containing silicate inclusions (a mixed analysis); data points that contain SiO_2 concentrations of over 200 ppm are excluded (Zack et al., 2004). There are a total of 88 data points collected from the Kuru-Vaara sample (57 from KV(1) and 31 from KV(2)), and 56 data points collected from the Gridino sample. Individual crystals are represented by a single data point (with the exception of crystal 37 in the Kuru-Vaara sample, from which four total data points were collected, making up a traverse across a single rutile crystal).

When data are collected, the uncertainty due to counting statistics is also calculated. The uncertainty, 1σ, is calculated as such (where the variable N stands for number of counts):

$$1\sigma = \frac{\sqrt{N}}{N}$$

In addition to the comparison of zirconium concentrations in the matrix versus in garnet, measurements of several rutile crystals within a single garnet crystal were taken. These rutile crystals, which exist at varying distances from the garnet core, are used as a traverse along the garnet to determine variability in zirconium concentrations. Similarly, a traverse along a single rutile crystal was taken to determine if zirconium concentrations in rutile vary depending on proximity to the rim or the core of the crystal.

Samples

The protolith of the eclogite samples from the Belomorian Province was basaltic oceanic crust (Shchipansky et al., 2012). The garnet crystals present within the samples contain inclusions of various minerals, such as quartz, mica, zircon, and rutile. Minerals present in the matrix are rutile, quartz, micas, omphacite, plagioclase, epidote, amphibole, and chlorite. EDS Spectra for amphibole and chlorite are present in Appendix A(e) and A(f) Sapphirine and spinel are absent from these samples. Two thin sections of the Kuru-Vaara sample were obtained (Figures 2(a) and 2(b)) which are: thin section KV(1) and thin section KV(2). KV(1) was used to obtain zirconium concentration measurements of the in-matrix rutile in Figure 5, and in the garnet traverse seen in Figure 6. The thin sections KV(1) and KV(2) were combined to obtain zirconium concentration measurements of the in-garnet rutile in Figure 5. The Gridino sample consists of one thin section, which was used to obtain zirconium concentration measurements for the graphs in Figure 5.

(a)

(b)

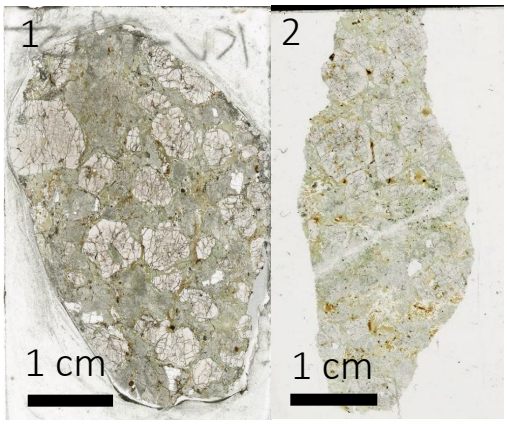

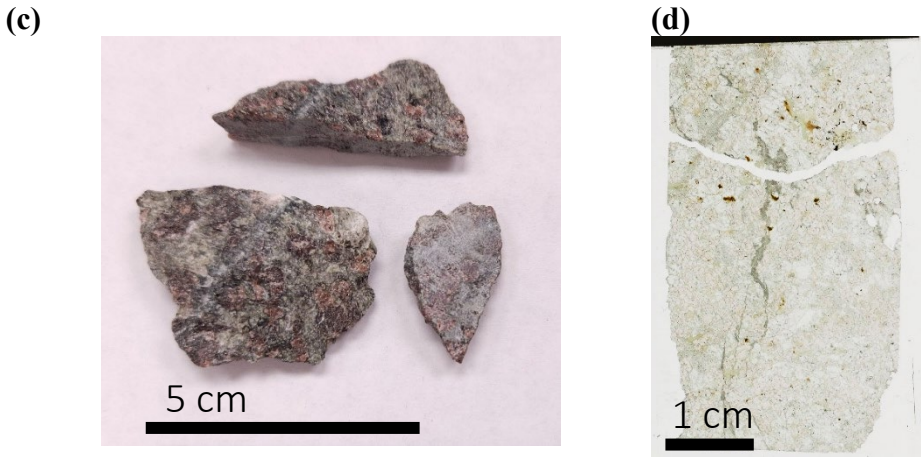

Fig 3. (a) Photograph of the Kuru-Vaara eclogite sample. (b) Scans of the two Kuru-Vaara thin sections. (c) Photograph of the Gridino eclogite sample. (d) Scans of the Gridino thin section.

Results

Multiple analyses of the zirconium content along a traverse of a single rutile crystal from the KV(1) thin section were analyzed. Figure 4 portrays this traverse of zirconium concentration measurements collected from this rutile crystal. The purpose of this traverse is to determine whether the crystal is uniform in its zirconium content. This graph shows that the crystal exhibits uniform concentrations within uncertainty. This indicates that there is no diffusion of zirconium into the surrounding matrix at this scale.

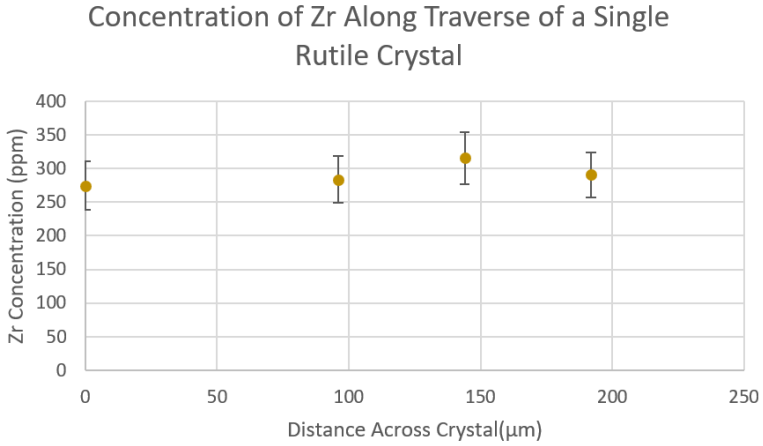

Fig 4. Zirconium concentration from a traverse along a single rutile crystal in KV(1). The data points are ordered by their distance across a single crystal, beginning at the crystal's rim at 0 μm.

Figure 5(a) is a plot of the zirconium concentrations of rutile crystals within the Kuru-Vaara sample, while graph 5(b) plots zirconium concentration results for rutile crystals within the Gridino sample. The rutile crystals within each sample were numbered 1-60, as can be seen labelled on the x-axis. These data points are separated into two populations: rutile crystals included

in garnet and rutile crystals in the matrix. The data are then processed using the mean-max method, following the procedure outlined in Harvey et al. (2021). Using the mean-max method, the four highest zirconium concentrations are averaged, and the standard deviation from these four values is used to determine an uncertainty envelope at 2σ (which has been labelled using the orange field on figures 5(a) and 5(b)). The purpose of using the four highest values is to determine the maximum concentrations reached, while also avoiding issues that may arise when using a singular data point as the maximum concentration value. The use of four data points is commonly used in other applications, such as detrital zircon geochronology (Harvey et al., 2021). For the Kuru-Vaara sample, the average concentrations that were determined using the mean-max method are: 753 ± 230 ppm for rutile crystals included within garnet, and 607 ± 68 ppm for rutile crystals within the matrix. For the Gridino sample, the average concentrations that were determined using the mean-max method are: 1046 ± 311 ppm for rutile crystals included within garnet, and 539 ± 301 ppm for rutile crystals within the matrix.

Graphs 5(c) and 5(d) display the zirconium concentrations of rutile crystals as box-and-whisker plots. When using a box-and-whisker plot, the upper quartile values can be used as the maximum zirconium concentration, as has been practiced in previous literature (Harvey et al., 2021). When compared to peak concentration values determined using the mean-max method, the values determined using box plots are comparable. Using the upper quartile value, the maximum zirconium concentrations for the Kuru-Vaara sample was determined to be: 572 ppm for rutile crystals included within garnet, and 533 ppm for rutile crystals within the matrix. For the Gridino sample, the maximum zirconium concentrations were determined to be: 669 ppm for rutile crystals included within garnet, and 382 ppm for rutile crystals within the matrix.

(a)

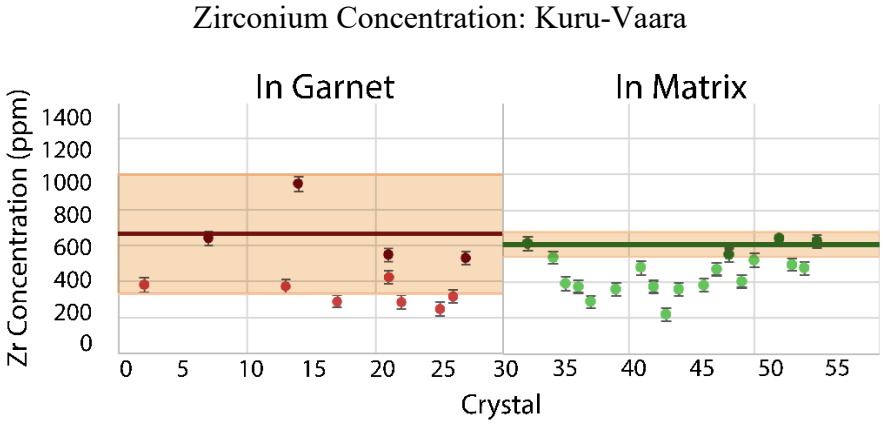

(b)

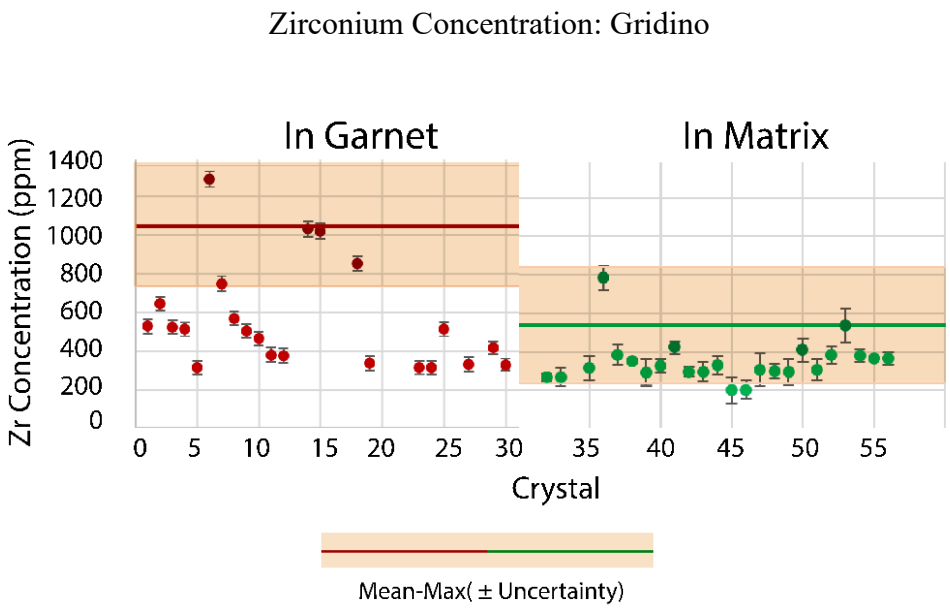

(c)

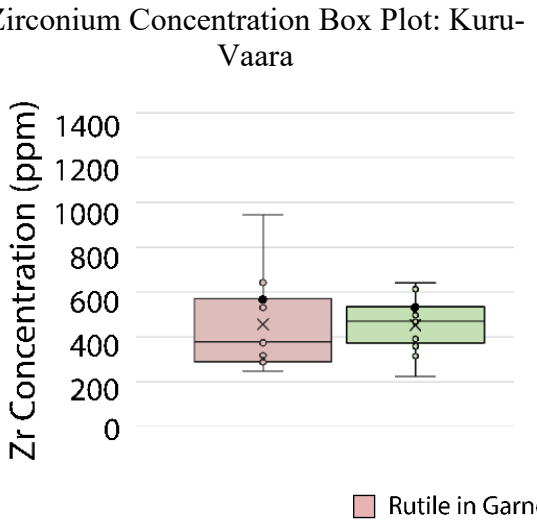

(d)

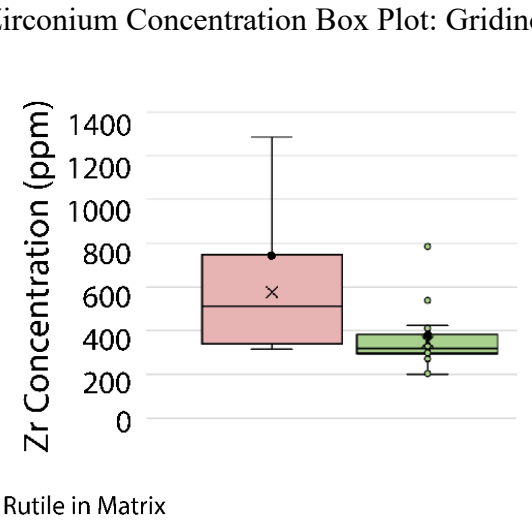

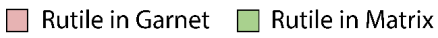

Fig 5. Graphs depicting the zirconium concentrations measured for each rutile crystal. Plotted using: **(a)** Mean-max method for Kuru-Vaara sample, yields mean-max value of 753 ± 230 ppm for within garnet and 607 ± 68 ppm (all uncertainties are calculated to 2σ) within matrix; **(b)** Mean-max method for Gridino sample, yields mean-max value of 1046 ± 311 ppm within garnet and 539 ± 301 ppm within matrix; **(c)** Box plot for Kuru-Vaara sample; yields upper quartile value of 572 ppm within garnet and 533 ppm within matrix; **(d)** Box plot for Gridino sample; yields upper quartile value of 669 ppm within garnet 382 ppm within matrix.

Multiple rutile crystal inclusions within a garnet from the core of the garnet crystal to its rim were analyzed using a garnet crystal in the KV(2) thin section. These data points are depicted

in Figure 6. The purpose of this traverse is to investigate whether zirconium concentration varies in rutile crystals in different parts of the garnet crystal. This is to assess whether changes in temperature are recorded over the growth history of a garnet crystal. In Figure 6, there is a decrease of zirconium concentration outside of uncertainty with increasing distance from core, which suggests that the garnet has grown along a path of decreasing temperature.

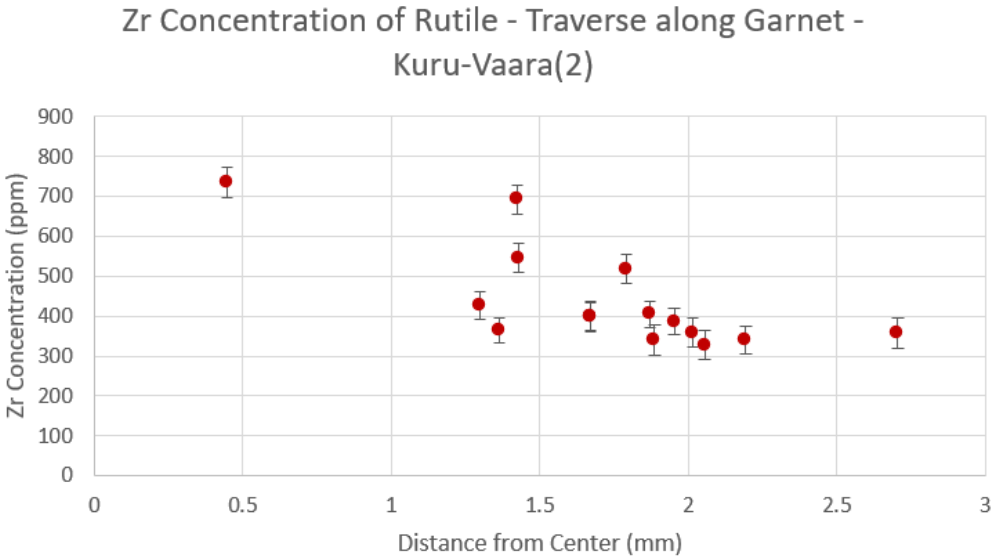

Fig 6. Zirconium concentration measurements from rutile crystal inclusions within a garnet crystal from KV(2). The data points are ordered by the measurement's distance from the core of the garnet crystal.

The garnet x-ray maps in Figure 7 depict the concentrations of iron, magnesium, manganese, calcium, and yttrium to map out the spatial distribution of major and minor elements in the garnet from Figure 6. The purpose of these maps is to determine zonation within the garnet. The garnet crystal exhibits a core enriched in manganese and iron, and a rim enriched in magnesium. The maps of calcium and yttrium do not exhibit any systematic differences in concentration from core to rim.

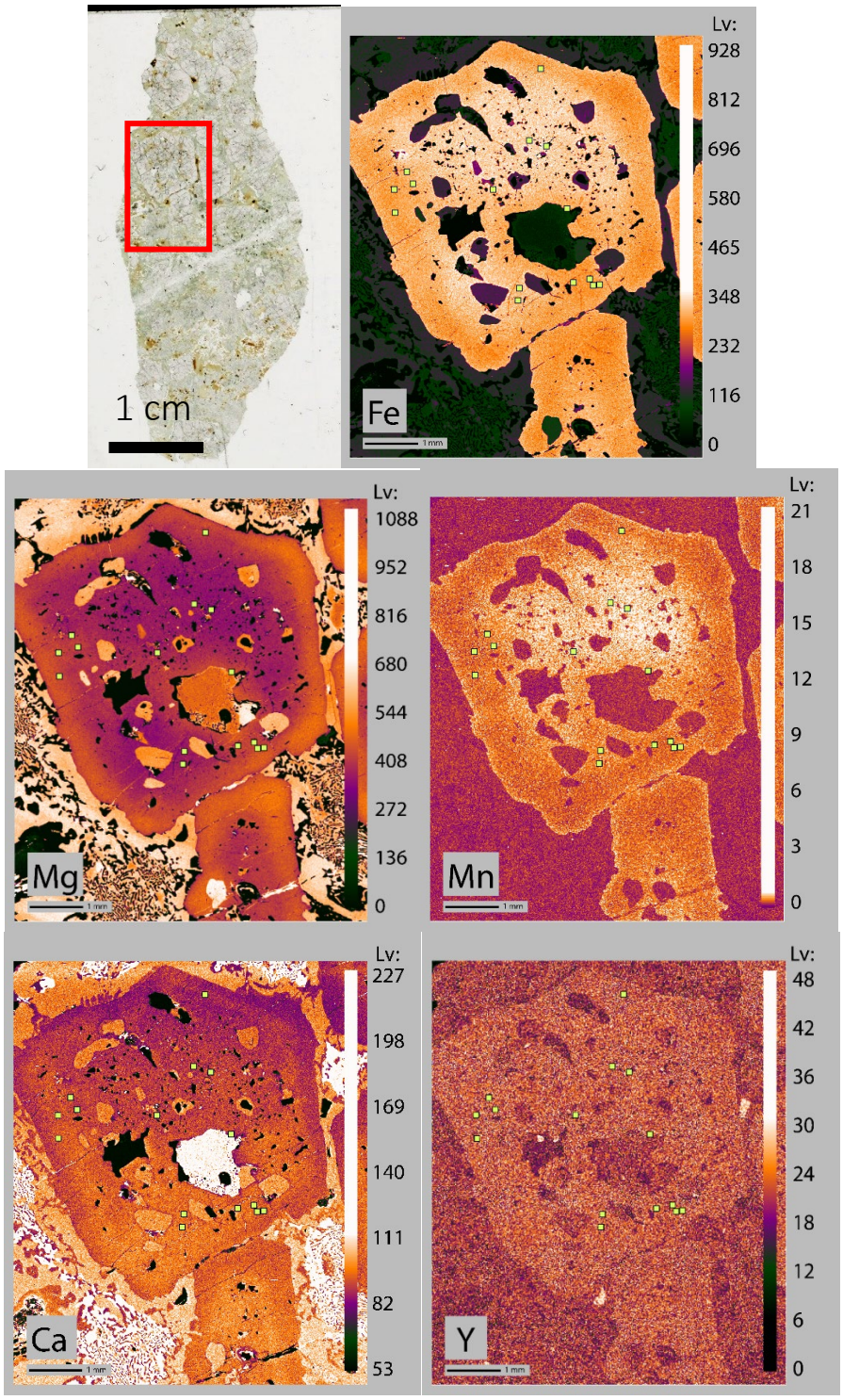

Fig 7. Garnet x-ray maps, with concentrations (from low to high) indicated by the colors: black, purple, orange, and white. The locations of rutile crystals used for Figures 6 and 9 are labelled using green squares. Included is a scan of KV (2), with mapped area outlined in red.

Discussion

Zirconium-in-Rutile Geothermometry

Figure 8 contains the temperature estimates for the Kuru-Vaara and Gridino sample that were obtained using the zirconium-in-rutile geothermometer. The zirconium concentrations, and therefore temperature estimates, of rutile crystals within garnets and within the matrix of both the Kuru-Vaara sample (Figure 8(a)) and the Gridino sample (Figure 8(b)) do not vary outside of uncertainty at the 2σ level. This result supports the null hypothesis that there is no difference in zirconium concentrations between these two sampled populations.

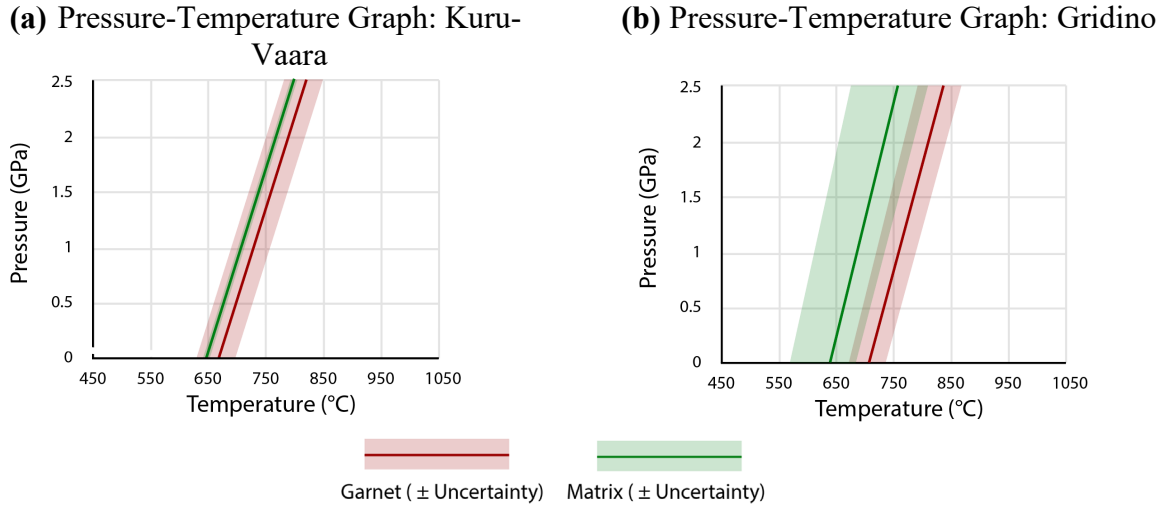

Fig 8. Results of zirconium-in-rutile geothermometry using zirconium concentration obtained by the mean-max method, and 2σ uncertainty. **(a)** Temperature estimates for the Kuru-Vaara sample over a wide range of pressures. **(b)** Temperature estimates for the Gridino sample over a wide range of pressures.

Garnet Traverse

Figure 9(a) depicts the same garnet traverse data that was plotted in Figure 6, which is a traverse within a garnet crystal in the thin section KV(1). A line calculated using linear regression has been fit onto the data. This line demonstrates the decreasing concentration of zirconium that occurs with increasing distance of the rutile crystal from the core of the garnet. This decreasing zirconium concentration suggests that the garnet recorded decreasing temperature throughout its growth.

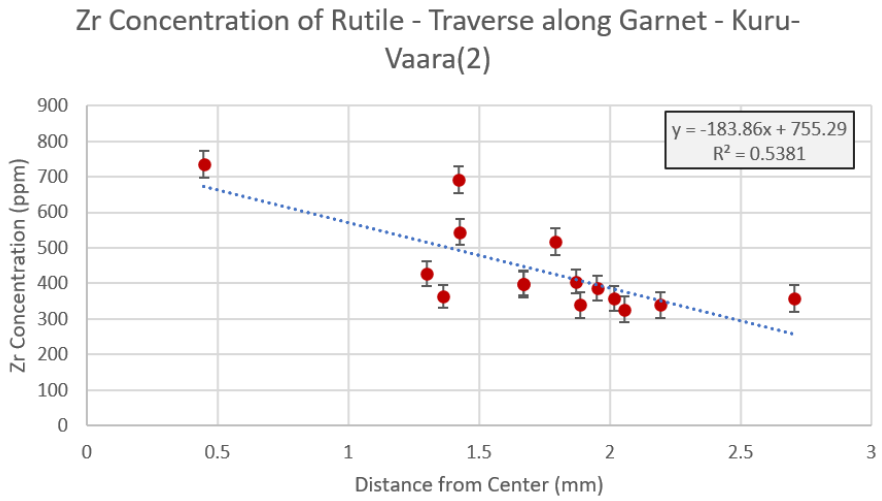

Fig 9. Garnet Traverse as seen in Figure 6 with the inclusion of a linear regression model.

Interpretation

The lack of variation outside of uncertainty between the zirconium concentrations of the two sampled populations in both Kuru-Vaara and Gridino supports the null hypothesis. This result suggests that the eclogite unit did not record exhumation temperatures that were any different from subduction zone temperatures. Additionally, the trend of zirconium concentration in rutile inclusions in garnet was found to decrease from garnet core to rim (as is seen in Figure 9), which suggests an overall decrease in temperature during garnet crystallization.

There are some possible explanations for the observed lack of variation between the two populations in the samples. One explanation may be that the rock may not have recorded high temperatures during its path back to the surface of the Earth. In Liu et al. (2017), the minerals sapphirine and spinel were used as a geothermometer to determine that these rocks experienced high-temperature conditions during exhumation. These minerals were not present in this sample, which also suggests that the rock does not record high exhumation temperatures. Another possible explanation is that the rocks were exhumed too quickly for high temperatures to be recorded. This can also explain the absence of the minerals sapphirine and spinel in these thin sections. A third reason may be that the exhumation temperatures recorded by these rocks were similar enough to subduction zone temperatures, and happened to not vary outside of uncertainty. However, this would contradict metamorphic path estimations by previous literature, namely Liu et al. (2017), which predicts high temperatures during exhumation.

Prograde vs. Retrograde Conditions

In Figure 10, the calculated zirconium-in-rutile geothermometry results are superimposed on top of the P-T diagram created by Liu et al. (2017) that plots the P-T paths of several different rock samples, including samples originating from the Kuru-Vaara and Gridino complexes. The calculated Kuru-Vaara isopleths intersect with the P-T path for Kuru-Vaara twice: once during the prograde path, and once during the retrograde path. The intersection of the calculated isopleth with the prograde path of the Kuru-Vaara sample is useful when arguing in support of the idea that these rocks record prograde path temperatures, as the calculations intersect with expected pressures and temperatures calculated by previous literature. Alternatively, in support of the argument that these

rocks instead record retrograde conditions rather than prograde conditions (as is implied by the garnet traverse in Figures 6 and 9), the isopleth intersects with the Kuru-Vaara sample's retrograde path estimated by Liu et al. (2017). Similarly, estimated Gridino isopleths intersect with previously calculated retrograde P-T paths for other Gridino samples (Perchuk & Morgunova, 2014). The growth of a garnet crystal during the rock's retrogression, rather than its subduction, is possible and has been seen in other subduction zone rocks (Jiao et al., 2021). Belomorian Province eclogites are known to have previously experienced ultrahigh-pressure conditions, however, the uncertainty of the Gridino sample's isopleth creates a large overlap with the prograde path estimated by Perchuk & Morgunova (2014) for the Gridino sample (Shchipansky et al., 2012). These prograde path conditions would be better constrained with the use of an additional geobarometer. Notably, none of these zirconium-in-rutile populations record the highest temperature conditions that were interpreted for the Kuru-Vaara sample by Liu et al. (2017), which were estimated due to the minerals sapphirine + spinel + plagioclase (sapphirine and spinel are not found in the samples studied).

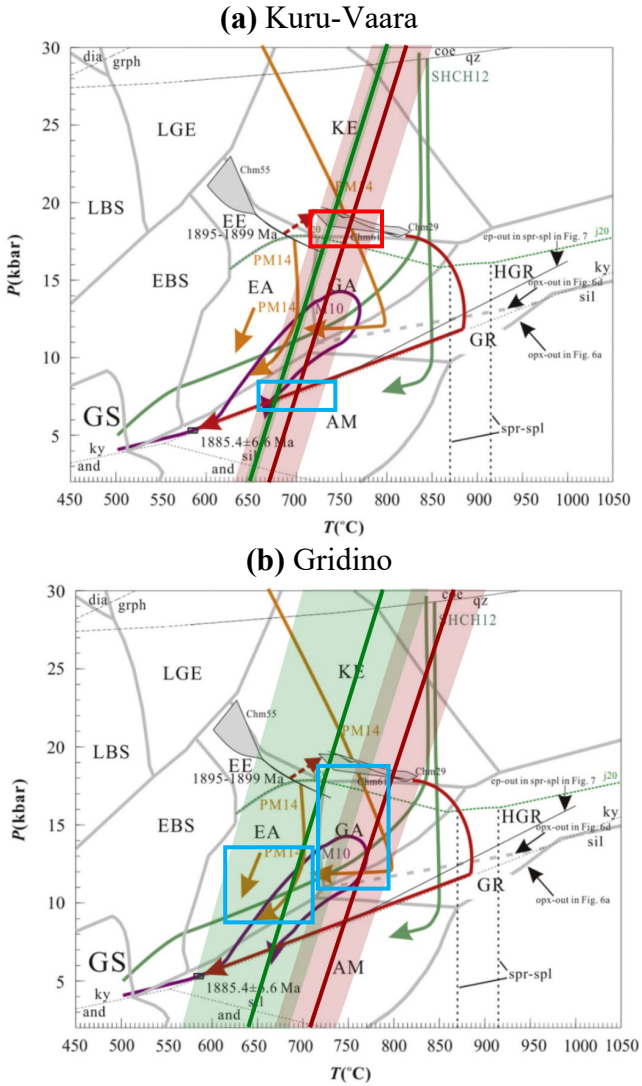

Fig 10. Zirconium-in-rutile geothermometry results superimposed onto P-T diagram from Liu et al. (2017). **(a)** Kuru-Vaara geothermometry results superimposed on top of the Kuru-Vaara P-T path

estimated by Liu et al. (2017) (red arrow and grey area). Intersections are labelled with colored outlines (red outline indicates overlap with prograde path, blue outline indicates overlap with retrograde path). **(b)** Gridino geothermometry results superimposed on top of the P-T diagram created by Liu et al. (2017), which includes pressure temperature paths for Gridino estimated by Perchuk & Morgunova (2014) (orange arrows). Intersections are labelled with blue outlines indicating an overlap with the retrograde path.

Figure 11 shows the isopleths from both the Kuru-Vaara and the Gridino sample plotted on top of a graph depicting P-T estimates from recent blueschists and eclogites throughout the globe. Though the Kuru-Vaara and Gridino isopleths exist at the high-end of these estimates, they still fall within the expected range of modern subduction zone rocks.

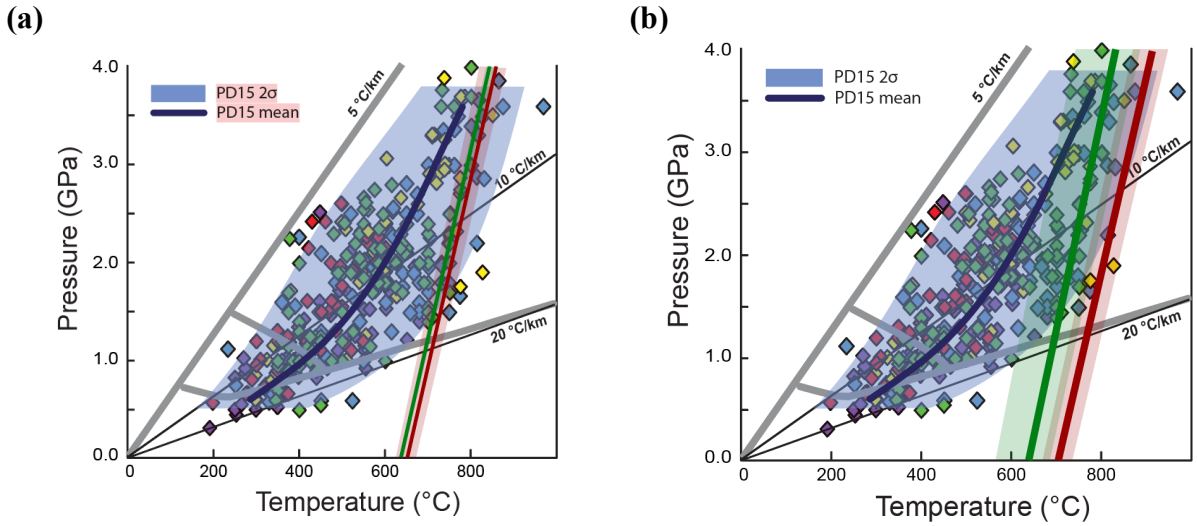

Fig 11. Zr-in-rutile isopleths from **(a)** Kuru-Vaara and **(b)** Gridino plotted on top of compilation of global P-T estimates from Penniston-Dorland et al. (2015).

Potential for Future Work

Neither of the two eclogite samples studied from this ancient subduction zone yield a difference in zirconium concentration between rutile crystals in the matrix and included within garnet. It would be worthwhile to further investigate the differences in zirconium concentration, and recorded temperature, between these two rock samples.

Kuru-Vaara eclogite samples contain evidence of preserved retrograde metamorphism in a garnet crystal. This creates a question as to whether the rutile crystals preserve zirconium concentrations reflective of the rock's prograde path, or its retrograde path. In the future, pairing these investigations with a geobarometer would aid in determining the P-T conditions this rock records, and its place along its P-T path.

Finally, there are limitations when it comes to the approach used in this investigation. Particularly, treating the entirety of a garnet crystal as a population may not serve as an accurate representation of the conditions under which the garnet formed. The different zones within a garnet represent different stages of garnet growth and therefore will record different environmental conditions. This limitation can be addressed using a garnet traverse to identify these environmental

conditions, but a more appropriate approach would likely be to treat different garnet zones individually, rather than as a single population.

Conclusions and Broader Impact

The two rock samples both support the null hypothesis that states that the two sampled populations will not exhibit differences in zirconium concentrations. Additionally, in the Kuru-Vaara sample, rutile crystal inclusions that exist along the traverse of a single garnet exhibit decreasing zirconium concentrations with increasing distance from the core. This indicates that the garnet crystal experienced high temperatures during the formation of its core, and lower temperatures during the formation of its rim. Using the comparisons to literature as seen in Figure 10, both prograde and retrograde conditions are feasible based on P-T paths estimated by Li et al (2017) and Perchuk & Morgunova (2014). Further research that includes the use of a geothermometer in addition to not treating inclusions within garnet as a single population may provide a more insightful result.

When making comparisons to previously estimated P-T paths, there is no evidence that these rocks experienced the high-temperature retrograde conditions predicted on these paths; rather, these calculated temperature conditions correlate with either an earlier stage on the rock's prograde path, or a later stage of its retrograde path. This is especially true for the Kuru-Vaara sample, where the highest temperatures recorded by zirconium in rutile are around 800 °C, while peak temperature conditions during retrogression estimated by Liu et al. (2017) reach 870-915°C.

Previous research, namely Brown et al. (2022) has proposed that ancient subduction zone environments were higher in temperature than modern subduction zones. However, as was shown in Figure 11, the Belomorian Province eclogite P-T estimates still fall within values expected of modern eclogites. Overall, further research on the Belomorian province and comparisons between different eclogite samples will allow for a deeper understanding not only of this ancient subduction zone, but also the changes in Earth's tectonic processes over time.

Acknowledgements

I would like to thank Dr. Sarah Penniston-Dorland for advising me and providing guidance for this project, Dr. Igor Puchtel for providing the two samples from Russia, and Dr. Phil Piccoli for the setup and operation of the EPMA for the analysis of samples. I would also like to thank Kate Bickerstaff, Dr. Christiana Hoff, and Kathy Stepien for their feedback and assistance.

Bibliography

Brown, M., Johnson, T., & Spencer, C. J. (2022). Secular changes in metamorphism and metamorphic cooling rates track the evolving plate-tectonic regime on Earth. *Journal of the Geological Society*, *179*(5), jgs2022-050.

Harvey, K. M., Penniston-Dorland, S. C., Kohn, M. J., & Piccoli, P. M. (2021). Assessing P-T variability in mélange blocks from the Catalina Schist: Is there differential movement at the subduction interface?. *Journal of Metamorphic Geology*, *39*(3), 271-295.

Jiao, S., Evans, N. J., Guo, J., Fitzsimons, I. C., Zi, J. W., & McDonald, B. J. (2021). Establishing the PT path of UHT granulites by geochemically distinguishing peritectic from retrograde garnet. *American Mineralogist*, *106*(10), 1640-1653.

Kohn, M. J. (2020). A refined zirconium-in-rutile thermometer. *American Mineralogist*, *105*(6), 963-971.

Li, X., Zhang, L., & Bader, T. (2020). The metamorphic PT history of Precambrian Belomorian eclogites (Shirokaya Salma), Russia. *Journal of Metamorphic Geology*, *39*(3), 363-389.

Liu, F., Zhang, L., Li, X., Slabunov, A. I., Wei, C., & Bader, T. (2017). The metamorphic evolution of Paleoproterozoic eclogites in Kuru-Vaara, northern Belomorian Province, Russia: Constraints from PT pseudosections and zircon dating. *Precambrian Research*, *289*, 31-47.

Penniston-Dorland, S. C., Kohn, M. J., & Manning, C. E. (2015). The global range of subduction zone thermal structures from exhumed blueschists and eclogites: Rocks are hotter than models. *Earth and Planetary Science Letters*, *428*, 243-254.

Perchuk, A. L., & Morgunova, A. A. (2014). Variable P–T paths and HP-UHP metamorphism in a Precambrian terrane, Gridino, Russia: Petrological evidence and geodynamic implications. *Gondwana Research*, *25*(2), 614-629.

Shchipansky, A. A., Khodorevskaya, L. I., & Slabunov, A. I. (2012). The geochemistry and isotopic age of eclogites from the Belomorian Belt (Kola Peninsula): evidence for subducted Archean oceanic crust. *Russian Geology and Geophysics*, *53*(3), 262-280.

Slabunov, A. I., Balagansky, V. V., & Shchipansky, A. A. (2021). Mesoarchean to Paleoproterozoic crustal evolution of the Belomorian Province, Fennoscandian Shield, and the tectonic setting of eclogites. *Russian Geology and Geophysics*, *62*(5), 525-546.

Syracuse, E. M., van Keken, P. E., & Abers, G. A. (2010). The global range of subduction zone thermal models. *Physics of the Earth and Planetary Interiors*, *183*(1-2), 73-90.

van Keken, P. E., Wada, I., Abers, G. A., Hacker, B. R., & Wang, K. (2018). Mafic high-pressure rocks are preferentially exhumed from warm subduction settings. *Geochemistry, Geophysics, Geosystems*, *19*(9), 2934-2961.

Zack, T., Moraes, R. D., & Kronz, A. (2004). Temperature dependence of Zr in rutile: empirical calibration of a rutile thermometer. *Contributions to Mineralogy and Petrology*, *148*, 471-488.

Appendices

Appendix A – EDS Spectra

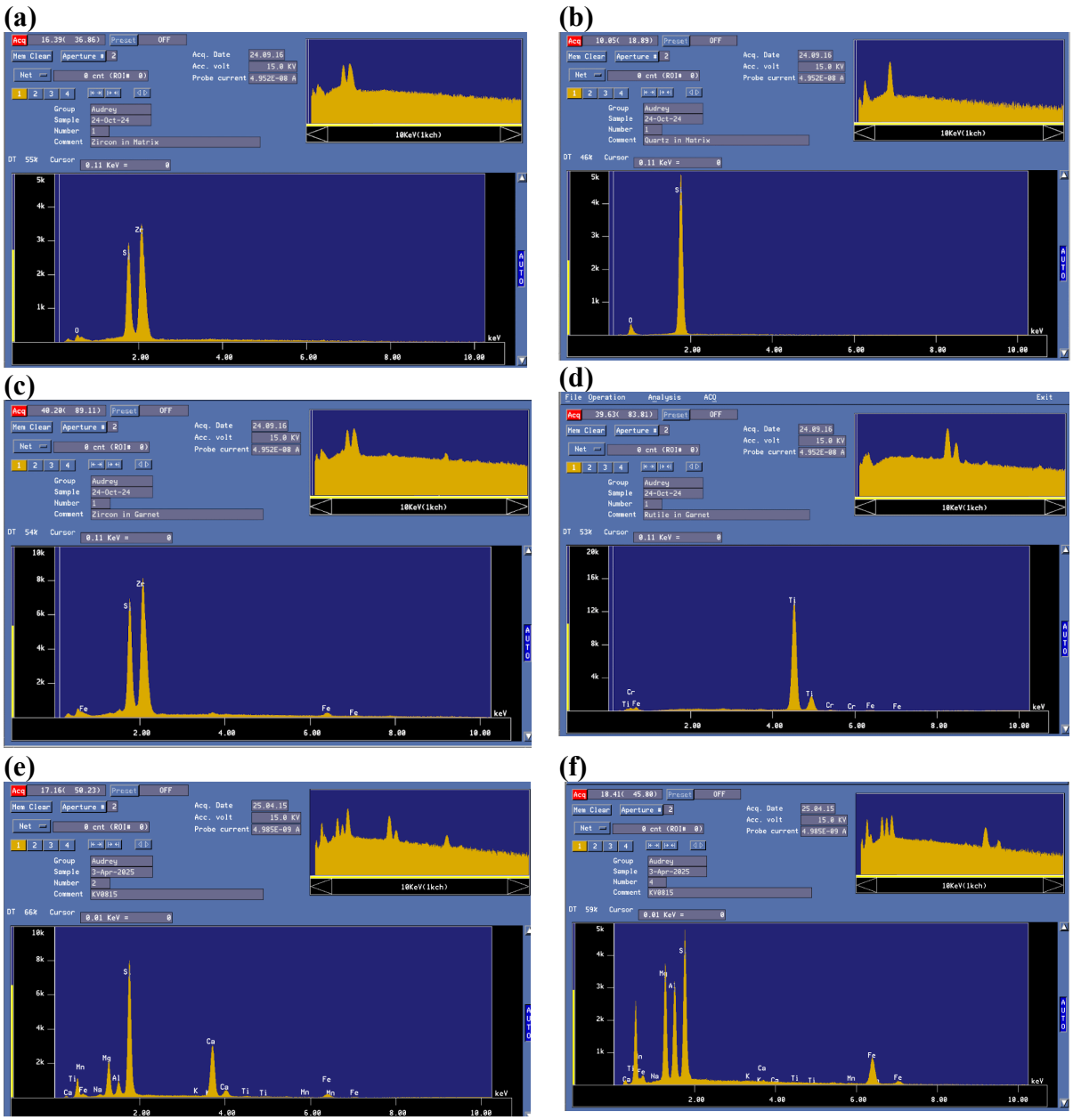

Appendix A. Thin Section KV(1): **(a)** EDS Spectra of zircon in matrix . **(b)** EDS Spectra of quartz in matrix. **(c)** EDS Spectra of zircon in garnet. **(d)** EDS Spectra of rutile in garnet. Thin section KV(2): **(e)** EDS Spectra of amphibole in matrix. **(f)** EDS Spectra of chlorite in matrix.

Appendix B – Summary Table

Summary table of filtered data collected by the EPMA.

(a) Kuru-Vaara – KV(1)

Garnet			**Matrix**		
		Uncertainty (2σ)			Uncertainty (2σ)
Crystal no.	Zr(ppm)	Zr(ppm)	Crystal no.	Zr(ppm)	Zr(ppm)
7	642	37	29	466	40
13	374	38	32	614	39
14	945	39	34	536	34
17	290	35	35	391	38
21	425	38	36	376	36
21	549	36	37	275	36
22	287	39	37	284	35
25	249	38	37	315	39
26	318	36	37	291	33
27	531	37	39	359	38
			41	481	36
			42	373	36
			43	222	34
			44	359	38
			46	384	35
			47	472	38
			48	551	37
			49	405	36
			50	522	37
			52	640	37
			53	497	33
			54	478	35
			55	626	38
			63	287	36

(b) Kuru-Vaara – KV(2)

Garnet		
		Uncertainty (2σ)
Crystal no.	Zr (ppm)	Zr(ppm)
7	734	38
12	427	35
18	364	32
16	692	36
17	545	36
20	398	37
21	400	35
22	518	36

23	405	33
30	340	37
25	387	34
28	358	36
29	327	36
31	340	36
27	357	38

(c) Gridino

Garnet			**Matrix**		
		Uncertainty (2σ)			Uncertainty (2σ)
Crystal no.	Zr(ppm)	Zr(ppm)	Crystal no.	Zr(ppm)	Zr(ppm)
1	529	38	32	270	34
2	643	36	33	270	33
3	524	36	35	317	36
4	512	36	36	785	38
5	315	34	37	386	36
6	1285	40	38	351	39
7	747	38	39	293	34
8	569	37	40	328	39
9	503	35	41	423	37
10	464	35	42	297	37
11	381	38	43	298	35
12	378	39	44	333	38
14	1030	41	45	201	37
15	1018	39	46	203	34
18	850	39	47	307	37
19	338	36	48	301	36
23	316	33	49	295	33
24	314	36	50	409	36
25	514	37	51	307	35
27	331	36	52	383	34
29	418	34	53	538	36
30	329	33	54	380	35
31	883	39	55	367	34
			56	366	36

Appendix C – Data

KV(1)

Crystal no.	No.	TiO2	ZrO2	Al2O3	FeO	Nb2O5	SiO2	Cr2O3	MnO	Ta2O5	Total	Comment	ppm of Zr
0	4.000	98.142	0.036	0.112	0.442	0.122	-0.022	0.208	0.008	0.044	99.092	RUT K13-0	264
0	5.000	96.975	0.039	0.127	0.456	0.136	-0.009	0.211	0.021	-0.042	97.912	RUT K13-0	287
0	6.000	98.533	0.035	0.118	0.466	0.089	-0.016	0.195	0.010	0.024	99.453	RUT K13-0	257
0	7.000	98.304	0.035	0.127	0.463	0.109	-0.020	0.136	0.024	0.078	99.256	RUT K13-0	259
0	8.000	98.482	0.039	0.134	0.448	0.132	-0.017	0.190	0.022	-0.077	99.353	RUT K13-0	290
0	9.000	98.252	0.038	0.146	0.363	0.148	-0.014	0.181	0.017	-0.032	99.099	RUT K13-0	281
0	10.000	98.358	0.033	0.251	0.411	0.120	-0.014	0.229	0.017	0.012	99.417	RUT K13-0	241
2	57.000	98.703	0.052	0.114	0.451	0.022	-0.003	0.798	0.024	-0.030	100.131	KV-O815 R	383
4	55.000	96.289	0.063	0.225	0.316	0.016	0.150	1.919	0.010	-0.045	98.941	KV-O815 R	468
5	56.000	98.668	0.063	0.211	0.502	0.037	0.099	0.741	0.008	-0.063	100.267	KV-O815 R	469
7	52.000	99.186	0.087	0.153	0.354	0.022	0.010	0.243	0.014	-0.032	100.036	KV-O815 R	642
8	53.000	97.517	0.096	0.207	0.353	0.036	0.172	0.901	0.026	0.013	99.321	KV-O815 R	707
13	58.000	99.607	0.051	0.119	0.465	0.022	-0.002	0.204	-0.007	-0.073	100.385	KV-O815 R	374
14	49.000	98.343	0.128	0.124	0.349	0.030	-0.010	0.527	-0.002	-0.022	99.467	KV-O815 R	945
15	54.000	98.416	0.063	0.173	0.731	0.003	0.117	0.478	0.013	0.030	100.023	KV-O815 R	466
16	59.000	98.161	0.079	0.287	0.309	0.030	0.193	0.536	-0.010	0.017	99.602	KV-O815 R	583
17	33.000	99.566	0.039	0.128	0.724	0.036	-0.010	0.356	0.036	-0.004	100.871	KV-O815 R	290
21	34.000	99.887	0.057	0.115	0.282	0.007	-0.015	0.180	0.016	-0.075	100.453	KV-O815 R	425
21	35.000	99.603	0.074	0.131	0.379	0.012	-0.010	0.133	0.031	0.049	100.402	KV-O815 R	549
22	31.000	98.423	0.039	0.124	0.271	0.042	0.009	1.085	-0.001	-0.084	99.908	KV-O815 R	287
25	32.000	99.243	0.034	0.156	0.491	-0.007	0.019	0.302	-0.019	0.007	100.226	KV-O815 R	249
26	30.000	98.295	0.043	0.109	0.360	0.014	-0.006	0.639	-0.024	-0.024	99.405	KV-O815 R	318
27	36.000	98.680	0.072	0.149	0.439	0.024	-0.001	0.220	0.026	0.043	99.652	KV-O815 R	531
28	37.000	99.169	0.089	0.199	0.518	0.035	0.074	0.168	-0.001	0.010	100.260	KV-O815 R	658
29	38.000	98.753	0.063	0.132	0.415	0.028	-0.001	0.464	0.051	0.034	99.939	KV-O815 R	466
31	39.000	98.763	0.119	0.145	0.502	-0.002	0.046	0.071	0.025	-0.012	99.656	KV-O815 R	877
32	40.000	99.555	0.083	0.125	0.623	0.051	-0.003	0.058	0.053	0.011	100.556	KV-O815 R	614
34	41.000	99.177	0.072	0.155	0.856	0.018	0.047	0.143	0.020	-0.040	100.447	KV-O815 R	536
35	28.000	99.689	0.053	0.115	0.055	0.045	-0.014	0.281	-0.009	0.009	100.223	KV-O815 R	391
36	29.000	98.951	0.051	0.105	0.187	0.055	-0.009	0.249	0.011	-0.061	99.539	KV-O815 R	376
37	12.000	94.760	0.042	0.096	0.190	0.059	0.009	0.380	-0.012	-0.025	95.500	Line 1 KV-0	309

Crystal no.	No.	TiO2	ZrO2	Al2O3	FeO	Nb2O5	SiO2	Cr2O3	MnO	Ta2O5	Total	Comment	ppm of Zr
37	13.000	99.004	0.037	0.106	0.147	0.014	0.002	0.383	0.007	-0.041	99.658	Line 2 KV-0	275
37	14.000	95.270	0.039	0.172	0.152	0.028	0.084	1.256	-0.002	-0.062	96.936	Line 3 KV-0	285
37	15.000	98.343	0.038	0.131	0.174	0.031	-0.004	0.340	-0.012	-0.043	98.998	Line 4 KV-0	284
37	16.000	98.369	0.043	0.145	0.130	0.040	0.024	0.912	-0.013	-0.061	99.588	Line 5 KV-0	315
37	17.000	98.995	0.039	0.144	0.165	0.027	0.013	0.404	0.010	-0.070	99.729	Line 6 KV-0	291
38	19.000	96.692	0.044	0.241	0.136	0.069	0.128	0.920	0.003	0.027	98.261	KV-O815 R	327
39	20.000	98.580	0.049	0.119	0.134	0.028	0.030	0.350	-0.017	-0.020	99.254	KV-O815 R	359
41	24.000	98.635	0.065	0.130	0.122	0.044	0.035	0.652	-0.007	0.032	99.707	KV-O815 R	481
42	25.000	99.021	0.050	0.137	0.084	0.054	0.015	0.650	0.012	-0.013	100.010	KV-O815 R	373
43	26.000	97.773	0.030	0.124	0.031	0.010	0.009	0.687	-0.006	-0.018	98.640	KV-O815 R	222
44	18.000	99.271	0.049	0.124	0.124	0.050	-0.012	0.311	-0.011	-0.038	99.868	KV-O815 R	359
46	21.000	99.986	0.052	0.101	0.190	0.048	-0.003	0.287	0.006	-0.066	100.600	KV-O815 R	384
47	22.000	99.507	0.064	0.115	0.240	0.114	-0.004	0.288	-0.046	0.040	100.317	KV-O815 R	472
48	23.000	98.974	0.074	0.120	0.250	0.067	0.006	0.377	0.026	-0.042	99.851	KV-O815 R	551
49	42.000	99.282	0.055	0.146	0.176	0.065	0.007	0.235	0.034	-0.028	99.970	KV-O815 R	405
50	43.000	99.463	0.071	0.132	0.206	0.100	0.050	0.434	-0.015	-0.012	100.428	KV-O815 R	522
51	44.000	96.769	0.084	0.113	0.185	0.049	0.022	0.468	-0.021	0.042	97.709	KV-O815 R	618
52	45.000	98.794	0.086	0.138	0.119	0.032	0.039	0.869	0.007	0.049	100.132	KV-O815 R	640
53	46.000	98.706	0.067	0.126	0.066	0.040	0.010	0.878	-0.006	0.016	99.904	KV-O815 R	497
54	47.000	98.279	0.065	0.127	0.131	0.055	0.031	0.883	-0.004	0.001	99.567	KV-O815 R	478
55	48.000	99.469	0.085	0.109	0.117	0.053	-0.005	0.456	0.006	-0.015	100.274	KV-O815 R	626
60	27.000	97.517	0.038	0.207	0.429	0.038	0.077	1.020	-0.017	-0.073	99.236	KV-O815 R	281
62	50.000	98.823	0.039	0.180	0.621	0.031	0.087	0.568	0.025	-0.027	100.347	KV-O815 R	287
63	51.000	99.011	0.039	0.118	0.480	0.047	-0.014	0.597	-0.022	-0.096	100.158	KV-O815 R	287

		Rel Unc (1	2sigma	Position (mm)	
Crystal no.	ppm of Si	ZrO2 (%) (	Zr (ppm)	X	Y
0	-101	6	32	78.914	54.307
0	-44	7	38	78.862	54.270
0	-76	6	33	78.799	54.290
0	-95	7	38	78.745	54.277
0	-78	6	37	78.633	54.382
0	-66	8	45	78.588	54.391
0	-63	8	37	78.523	54.433
2	-15	5	40	63.233	79.587
4	699	4	39	63.901	78.180
5	465	4	37	63.777	78.389
7	47	3	37	66.193	79.353
8	806	3	39	66.095	79.255
13	-8	5	38	62.311	80.995
14	-45	2	39	66.521	76.808
15	546	4	37	65.938	80.260
16	904	3	38	62.765	81.023
17	-48	6	35	70.243	67.624
21	-71	4	38	69.226	67.776
21	-46	3	36	70.017	69.832
22	41	7	39	71.866	68.433
25	90	8	38	71.438	68.429
26	-27	6	36	72.126	69.464
27	-4	3	37	70.017	69.832
28	345	3	39	69.969	69.785
29	-6	4	40	69.650	69.986
31	213	2	38	69.861	70.354
32	-13	3	39	70.060	70.453
34	217	3	34	69.452	70.535
35	-65	5	38	72.416	69.440
36	-42	5	36	72.239	69.356
37	42	6	37	80.400	60.369

Crystal no.	ppm of Si	Rel Unc (1 ZrO2 (%) (	2sigma Zr (ppm)	Position (mm) X	Y
37	10	7	36	80.445	60.352
37	393	7	41	80.490	60.336
37	-18	6	35	80.536	60.320
37	114	6	39	80.581	60.303
37	62	6	33	80.626	60.287
38	600	6	37	80.309	65.358
39	141	5	38	81.690	66.893
41	165	4	36	80.320	70.123
42	70	5	36	79.753	70.238
43	44	8	34	79.392	70.379
44	-58	5	38	75.281	63.679
46	-14	5	35	76.340	65.903
47	-21	4	38	76.284	66.106
48	26	3	37	75.914	65.876
49	31	4	36	71.404	80.491
50	232	4	37	70.007	80.831
51	103	3	38	70.333	81.915
52	180	3	37	70.117	81.946
53	47	3	33	69.795	82.002
54	144	4	35	69.583	81.998
55	-25	3	38	70.197	82.560
60	361	7	40	78.192	70.211
62	407	6	34	67.198	78.604
63	-67	6	36	67.235	78.896

KV(2)

Crystal	No.	TiO2	ZrO2	Al2O3	FeO	Nb2O5	SiO2	Cr2O3	MnO	Ta2O5	Total	Comment
1	60.000	98.218	0.079	0.133	0.872	0.043	0.060	0.341	0.032	0.008	99.785	KV0815 1
2	61.000	91.996	0.065	0.844	1.948	0.019	1.695	0.447	0.063	-0.072	97.004	KV0815 2
4	63.000	98.075	0.073	0.507	0.976	0.035	0.405	0.363	0.004	0.004	100.441	KV0815 4
3	62.000	99.789	0.066	0.113	0.740	0.044	0.048	0.312	0.015	-0.029	101.099	KV0815 3
5	64.000	99.230	0.055	0.114	0.735	0.007	0.044	0.615	0.032	0.029	100.860	KV0815 5
6	65.000	98.351	0.057	0.166	0.822	0.024	0.150	0.583	0.040	-0.048	100.145	KV0815 6
7	66.000	100.056	0.099	0.122	0.803	0.016	0.035	0.341	0.006	-0.002	101.475	KV0815 7
9	68.000	99.334	0.084	0.117	0.755	0.025	0.044	0.281	0.043	0.034	100.718	KV0815 9
8	67.000	98.884	0.062	0.119	0.758	0.030	0.054	0.369	-0.016	0.025	100.284	KV0815 8
10	69.000	97.119	0.086	0.382	1.217	0.051	0.590	0.401	0.010	-0.057	99.799	KV0815 10
13	72.000	99.105	0.070	0.138	0.921	0.020	0.062	0.355	0.005	0.026	100.701	KV0815 13
15	74.000	99.501	0.085	0.130	0.830	0.026	0.043	0.135	0.009	0.031	100.790	KV0815 15
12	71.000	98.999	0.058	0.110	0.874	0.055	0.042	0.397	0.016	0.014	100.563	KV0815 12
14	73.000	99.030	0.076	0.126	0.938	0.007	0.047	0.163	0.010	-0.064	100.334	KV0815 14
19	84.000	98.909	0.055	0.138	1.003	-0.001	0.082	0.457	0.023	0.041	100.708	KV0815 19
11	70.000	97.849	0.058	0.220	0.793	0.021	0.227	0.352	-0.021	-0.019	99.479	KV0815 11
18	83.000	98.534	0.049	0.108	0.766	0.035	0.040	0.552	0.015	-0.040	100.060	KV0815 18
16	75.000	99.404	0.093	0.119	0.881	0.029	0.041	0.173	-0.008	-0.004	100.728	KV0815 16
17	76.000	98.409	0.074	0.115	0.686	-0.001	0.000	0.492	0.022	-0.033	99.764	KV0815 17
20	85.000	98.770	0.054	0.100	0.539	0.018	0.000	0.652	0.029	0.018	100.181	KV0815 20
21	86.000	98.695	0.054	0.081	0.533	0.030	0.004	0.684	0.007	-0.036	100.050	KV0815 21
22	87.000	99.281	0.070	0.121	0.614	0.033	0.032	0.411	-0.009	-0.052	100.500	KV0815 22
23	88.000	98.796	0.055	0.125	0.707	0.024	0.029	0.478	-0.004	-0.022	100.188	KV0815 23
30	82.000	98.709	0.046	0.119	0.553	0.028	-0.002	0.423	0.014	-0.031	99.859	KV0815 30
24	89.000	90.739	0.053	1.151	1.909	0.025	2.335	0.514	0.020	0.025	96.770	KV0815 24
25	90.000	98.200	0.052	0.110	0.693	0.048	0.032	0.568	0.006	0.031	99.739	KV0815 25
28	79.000	99.579	0.048	0.105	0.624	-0.007	0.025	0.490	-0.006	-0.048	100.811	KV0815 28
29	80.000	97.518	0.044	0.088	0.515	0.011	-0.003	0.445	0.007	0.017	98.641	KV0815 29
31	81.000	99.376	0.046	0.108	0.591	-0.007	0.015	0.460	0.032	0.009	100.630	KV0815 31
26	77.000	99.316	0.077	0.169	0.867	0.033	0.103	0.144	0.030	-0.037	100.702	KV0815 26
27	78.000	99.813	0.048	0.104	0.610	0.014	0.010	0.288	0.001	-0.050	100.837	KV0815 27

			Uncertainty 2sigma,		in mm		
Crystal	ppm of Zr	ppm of Si	ZrO2	Zr ppm	X	Y	Z
1	3409	997854	3	35	17.989	49.187	10.651
2	4468	970042	4	37	18.040	49.077	10.650
4	3630	1004409	4	38	17.851	49.035	10.650
3	3118	1010985	4	36	17.832	49.057	10.651
5	6151	1008595	4	36	18.258	49.036	10.651
6	5831	1001454	4	37	18.272	49.032	10.651
7	3406	1014748	3	38	17.604	48.957	10.650
9	2810	1007182	3	37	17.227	49.146	10.651
8	3687	1002839	4	34	17.225	49.335	10.651
10	4013	997992	3	38	16.950	49.085	10.656
13	3552	1007011	4	38	17.753	50.265	10.653
15	1351	1007897	3	36	17.627	50.269	10.647
12	3973	1005633	4	35	17.843	50.478	10.649
14	1634	1003338	3	34	17.624	50.457	10.649
19	4571	1007082	4	36	19.325	49.208	10.653
11	3518	994788	4	35	17.782	50.521	10.649
18	5521	1000596	4	32	19.323	49.468	10.653
16	1732	1007276	3	36	16.745	49.878	10.646
17	4924	997642	3	36	16.689	49.777	10.648
20	6517	1001805	5	37	19.630	49.497	10.649
21	6835	1000504	4	35	19.630	49.497	10.649
22	4114	1005002	4	36	17.283	47.539	10.653
23	4781	1001880	4	33	17.546	47.369	10.655
30	4227	998586	5	37	19.353	50.490	10.650
24	5144	967699	5	38	17.567	47.314	10.655
25	5678	997385	4	34	17.600	47.274	10.653
28	4895	1008113	5	36	19.198	50.800	10.646
29	4446	986408	6	36	19.281	50.785	10.649
31	4602	1006301	5	36	19.363	50.897	10.649
26	1437	1007019	3	35	15.462	49.966	10.648
27	2875	1008373	5	38	15.384	49.916	10.646

Gridino

Crystal	No.	TiO2	ZrO2	Al2O3	FeO	Nb2O5	SiO2	Cr2O3	MnO	Ta2O5	Total	Comment
1	43.000	98.213	0.071	0.101	0.128	0.048	-0.015	0.393	-0.005	0.028	98.961	GRID 1
2	41.000	99.337	0.087	0.107	0.634	0.089	0.019	0.282	0.035	0.011	100.600	GRID 2
3	42.000	99.354	0.071	0.124	0.766	0.058	0.023	0.351	0.027	0.025	100.798	GRID 3
4	40.000	99.870	0.069	0.091	0.344	0.113	-0.004	0.151	-0.010	0.003	100.628	GRID 4
5	44.000	98.790	0.043	0.104	0.688	0.086	0.011	0.428	0.003	-0.012	100.140	GRID 5
6	45.000	99.530	0.174	0.085	0.337	0.044	-0.013	0.777	0.016	0.006	100.954	GRID 6
7	52.000	100.334	0.101	0.098	0.426	0.063	-0.008	0.260	0.011	-0.007	101.278	GRID 7
8	59.000	99.519	0.077	0.120	0.749	0.084	0.023	0.254	0.036	0.034	100.896	GRID 8
9	56.000	98.755	0.068	0.109	0.808	0.062	0.041	0.310	0.030	-0.113	100.070	GRID 9
10	57.000	99.047	0.063	0.125	0.912	0.063	0.027	0.312	0.004	-0.076	100.475	GRID 10
11	58.000	99.283	0.051	0.109	0.649	0.033	0.034	0.397	0.037	0.001	100.594	GRID 11
12	22.000	97.721	0.051	0.091	0.414	0.076	-0.005	0.333	0.002	-0.063	98.620	GRID 12
13	10.000	98.121	0.079	0.130	0.679	0.056	0.101	0.171	0.017	-0.031	99.322	GRID 13
14	11.000	99.310	0.139	0.108	0.720	0.101	0.036	0.209	0.034	0.042	100.699	GRID 14
15	12.000	98.666	0.138	0.098	0.692	0.050	0.013	0.261	-0.016	0.015	99.917	GRID 15
16	13.000	97.658	0.128	0.099	0.834	0.057	0.058	0.154	0.032	-0.112	98.907	GRID 16
17	14.000	97.314	0.083	0.126	0.930	0.058	0.053	0.237	0.022	-0.008	98.816	GRID 17
18	15.000	96.832	0.115	0.143	0.913	0.074	0.039	0.156	0.038	0.034	98.342	GRID 18
19	9.000	99.425	0.046	0.089	0.590	0.079	0.005	0.325	0.025	0.034	100.617	GRID 19
20	23.000	96.249	0.069	0.402	1.265	0.107	0.691	0.295	0.056	0.005	99.140	GRID 20
22	24.000	91.346	0.066	1.411	2.344	0.094	2.532	0.218	0.076	-0.029	98.057	GRID 22
23	28.000	99.064	0.043	0.096	0.497	0.073	-0.006	0.378	-0.010	-0.075	100.060	GRID 23
24	29.000	98.764	0.042	0.107	0.552	0.041	0.015	0.397	0.031	-0.007	99.942	GRID 24
25	39.000	99.916	0.069	0.089	0.353	0.091	-0.003	0.146	-0.009	-0.017	100.634	GRID 25
26	8.000	97.232	0.063	0.689	1.217	0.069	0.044	0.371	0.010	-0.033	99.661	GRID 26
27	33.000	99.326	0.045	0.099	0.390	0.060	-0.001	0.538	0.001	-0.046	100.413	GRID 27
28	38.000	99.190	0.047	0.148	0.781	0.056	0.072	0.424	0.013	0.023	100.753	GRID 28
29	37.000	98.845	0.057	0.109	0.714	0.076	0.020	0.429	0.032	0.020	100.301	GRID 29
30	6.000	99.452	0.045	0.101	0.603	0.070	0.008	0.426	0.001	0.053	100.757	GRID 30
31	7.000	98.487	0.119	0.124	0.981	0.052	0.052	0.164	0.023	-0.018	99.984	GRID 31
32	53.000	100.640	0.036	0.084	0.074	0.066	-0.004	0.277	-0.005	-0.007	101.161	GRID 32

Crystal	No.	TiO2	ZrO2	Al2O3	FeO	Nb2O5	SiO2	Cr2O3	MnO	Ta2O5	Total	Comment
33	54.000	100.174	0.036	0.113	0.268	0.075	0.011	0.239	0.033	-0.011	100.937	GRID 33
35	49.000	100.199	0.043	0.102	0.138	0.071	-0.014	0.298	0.037	-0.017	100.857	GRID 35
36	48.000	100.630	0.106	0.111	0.142	0.044	-0.014	0.211	-0.024	0.022	101.228	GRID 36
37	47.000	100.524	0.052	0.104	0.136	0.050	-0.011	0.244	-0.019	-0.029	101.051	GRID 37
38	50.000	100.351	0.047	0.107	0.062	0.062	0.000	0.257	0.022	-0.035	100.872	GRID 38
39	51.000	101.208	0.040	0.111	0.065	0.047	-0.015	0.315	-0.009	0.124	101.887	GRID 39
40	46.000	100.599	0.044	0.100	0.140	0.086	-0.007	0.272	-0.024	-0.074	101.134	GRID 40
41	55.000	100.448	0.057	0.098	0.181	0.065	-0.007	0.221	-0.031	-0.012	101.019	GRID 41
42	16.000	100.355	0.040	0.071	0.039	0.060	-0.005	0.357	0.006	-0.043	100.880	GRID 42
43	17.000	99.596	0.040	0.069	0.129	0.038	-0.011	0.396	-0.020	-0.017	100.220	GRID 43
44	18.000	100.347	0.045	0.083	0.037	0.054	-0.010	0.352	-0.007	0.047	100.949	GRID 44
45	19.000	99.079	0.027	0.072	0.221	0.044	-0.014	0.356	-0.008	-0.028	99.751	GRID 45
46	20.000	99.699	0.027	0.079	0.187	0.028	-0.010	0.385	-0.020	-0.081	100.294	GRID 46
47	21.000	98.613	0.041	0.073	0.038	0.044	-0.019	0.326	-0.027	-0.034	99.055	GRID 47
48	25.000	100.155	0.041	0.071	0.082	0.079	-0.008	0.345	0.025	0.004	100.792	GRID 48
49	26.000	100.422	0.040	0.077	0.091	0.050	-0.014	0.377	-0.012	0.024	101.056	GRID 49
50	27.000	98.578	0.055	0.101	0.117	0.075	-0.013	0.194	-0.016	0.002	99.093	GRID 50
51	36.000	100.105	0.042	0.091	0.098	0.057	-0.011	0.173	0.002	-0.026	100.531	GRID 51
52	34.000	100.349	0.052	0.099	0.063	0.086	-0.010	0.424	0.016	0.018	101.096	GRID 52
53	35.000	99.761	0.073	0.103	0.132	0.070	-0.019	0.422	-0.003	-0.053	100.484	GRID 53
54	30.000	100.237	0.051	0.109	0.155	0.070	-0.007	0.138	0.024	0.009	100.786	GRID 54
55	31.000	99.961	0.050	0.106	0.187	0.107	-0.001	0.178	0.022	0.059	100.668	GRID 55
56	32.000	99.862	0.049	0.106	0.130	0.069	-0.007	0.155	0.028	0.005	100.398	GRID 56

			Uncertainty		in mm		
Crystal	ppm of Zr	ppm of Si	ZrO2	Zr ppm	X	Y	Z
1	529	-69	4	38	54.209	59.181	10.634
2	643	87	3	36	53.434	63.545	10.625
3	524	108	3	36	53.388	63.406	10.627
4	512	-17	4	36	76.026	63.945	10.642
5	315	50	5	34	57.346	59.401	10.635
6	1285	-59	2	40	56.582	57.279	10.640
7	747	-38	3	38	51.487	53.142	10.640
8	569	109	3	37	51.890	45.786	10.653
9	503	192	3	35	53.737	45.705	10.659
10	464	125	4	35	53.680	45.710	10.657
11	381	160	5	38	53.629	45.671	10.656
12	378	-22	5	39	67.435	58.358	10.647
13	586	472	3	37	66.740	48.897	10.663
14	1030	168	2	41	66.441	49.166	10.654
15	1018	61	2	39	66.316	48.795	10.665
16	947	272	2	38	66.648	49.395	10.670
17	615	249	3	37	66.596	49.617	10.663
18	850	180	2	39	66.358	49.526	10.663
19	338	22	5	36	70.548	44.305	10.672
20	513	3229	4	36	69.744	58.421	10.649
22	485	11833	4	38	69.611	58.359	10.646
23	316	-26	5	33	78.066	57.922	10.651
24	314	70	6	36	78.066	57.922	10.651
25	514	-15	4	37	76.026	63.945	10.642
26	466	205	4	36	75.903	46.825	10.670
27	331	-3	6	36	82.483	52.283	10.665
28	346	337	5	38	83.622	59.667	10.653
29	418	94	4	34	83.720	59.548	10.656
30	329	36	5	33	81.541	44.009	10.682
31	883	243	2	39	81.484	43.971	10.675
32	270	-20	6	34	52.879	48.332	10.653

			Uncertainty		in mm		
Crystal	ppm of Zr	ppm of Si	ZrO2	Zr ppm	X	Y	Z
33	270	49	6	33	53.044	48.302	10.647
35	317	-64	6	36	57.610	53.817	10.646
36	785	-63	2	38	56.845	54.347	10.644
37	386	-52	5	36	56.178	54.160	10.641
38	351	-1	6	39	56.987	53.401	10.645
39	293	-69	6	34	56.927	53.202	10.642
40	328	-32	6	39	54.658	56.548	10.637
41	423	-34	4	37	56.583	49.153	10.656
42	297	-24	6	37	64.955	48.577	10.663
43	298	-50	6	35	63.787	47.857	10.663
44	333	-47	6	38	65.097	53.102	10.655
45	201	-65	9	37	66.141	53.846	10.653
46	203	-49	8	34	66.141	53.846	10.653
47	307	-86	6	37	65.228	56.811	10.646
48	301	-39	6	36	71.798	61.108	10.644
49	295	-66	6	33	71.798	61.108	10.644
50	409	-61	4	36	74.001	60.585	10.648
51	307	-53	6	35	85.610	58.745	10.660
52	383	-46	4	34	83.158	51.479	10.666
53	538	-89	3	36	83.760	50.032	10.673
54	380	-32	5	35	74.532	53.652	10.661
55	367	-7	5	34	74.532	53.652	10.661
56	366	-33	5	36	74.851	53.606	10.658

Appendix D – University Honor Code

I pledge on my honor that I have not given or received any unauthorized assistance on this examination/assignment.